Hollow Cathode Ion Lasers for Deep Ultraviolet Raman Spectroscopy and Fluorescence Imaging

M. C. Storrie-Lombardi
Jet Propulsion Laboratory, California Institute of Technology, Pasadena, California

W. F. Hug
Photon Systems, Inc., Pasadena, California

G. D. McDonald, A. I. Tsapin, and K. H. Nealson
Jet Propulsion Laboratory, California Institute of Technology, Pasadena, California

This article describes the development of hollow cathode ion lasers and their use in constructing an ultraviolet micro-Raman spectrograph with native fluorescence imaging capability. Any one of three excitation wavelengths can be chosen within seconds using flip mirrors and a dichroic mirror slide. Excitation at 224.3 nm is provided by a helium silver (HeAg) hollow cathode metal ion laser, at 248.6 nm by a neon copper (NeCu) hollow cathode metal ion laser, and at 325.0 nm by a helium cadmium (HeCd) positive column metal ion laser. Refractive microscope objectives focus quasi-cw laser light on a sample and collect 180° scattered photons. Imaging can be accomplished by either broadband excitation in visible wavelengths or by deep ultraviolet laser-induced excitation of native fluorescence in untagged microorganisms. This makes possible a detection strategy employing a rapid image scan with laser excitation to locate regions of native fluorescence activity, followed by deep ultraviolet resonance Raman spectroscopy of the identified fluorescent sites. We have employed this probe to explore non-destructive *in situ* detection of microorganisms in mineral and soil substrates. We present here the deep ultraviolet resonance Raman spectra for the gram negative iron reducing bacterium *Shewanella oneidensis* obtained while the microorganism remains *in situ* on the unpolished surface of the mineral calcite and in a Mars soil analog, JSC1. In the current configuration the *in situ* surface scanning limit of detection for fluorescence is one organism in 2×10^4 μ^2 field of view and of order 20-30 microorganisms for Raman spectra. For the Mars soil sample analog fluorescent target selection gives an effective ultraviolet resonance Raman spectral detection limit of 6×10^4 cells/gm or ~ 60ppb.

I. INTRODUCTION

Detection and identification of sparsely distributed yet spatially localized concentrations of organic material is a fundamental task common to *in situ* detection of life on Mars, planetary contamination containment, forensic investigation, and biological warfare countermeasures. The goals for each of these efforts are best accomplished with minimal sample preparation including the avoidance of tagging molecules. Amongst optical techniques, fluorescence remains the gold standard for sensitivity. However, as usually implemented it has either depended on the introduction of fluorescent tags or the serendipitous presence of a chromophore molecule with strong absorption bands at visible wavelengths. A variety of ring compounds including the aromatic amino acids and the nucleic acids exhibit strong native fluorescence response to excitation between 220 and 250 nm.

While native fluorescence response might admirably serve as an initial detection probe it often provides little specificity to aid in the identification of a target. Raman spectroscopy is a vibrational spectroscopy technique capable of producing spectra with a high information content. The efficiency of the technique increases as the fourth power of excitation frequency. If excitation occurs within the absorption band of a target molecule the ensuing resonance Raman event can enhance signal strength by as much as 10^6 to 10^8. The aromatic amino acids and nucleic acids exhibit strong resonance Raman cross-sections at 224 and 248 nm, respectively.

The routine use of aromatic amino acids and nucleic acids as biologically ubiquitous sources for eliciting native fluorescence and resonance Raman signatures has been dependent on the development of a lightweight laser light source emitting photons in the 220 to 250 nm range. We describe such lasers and discuss the native fluorescence and resonance Raman response of the aromatic amino and nucleic acids to excitation in the deep ultraviolet at 224.3 and 248.6 nm. We report the use of a combination of native fluorescence imaging and resonance Raman spectroscopy for the detection of spatially localized clusters of bacteria on a calcite surface and in a Mars soil analog.

Deep UV Hollow Cathode Sputtering Metal Ion Lasers – Hollow cathode metal ion lasers were first demonstrated at the University of Budapest in 1974.[1] The early development of these lasers was hampered by the lack of durable low scatter and low absorption laser mirror coatings resistant to optical damage. Recognized as an efficient source of deep UV laser light, the development of this technology continued at a handful of academic and industrial sites.[2-4] Recent advances in optical coating technology now makes commercial development of these lasers feasible.

Hollow cathode lasers have several unique properties that make them ideal for *in situ* UV laser induced fluorescence and Raman spectroscopy. Among these features are an array of emission wavelengths including 224.3 nm from a helium charge exchange pumped sputtering silver hollow cathode laser and 248.6, 260.0 and 270.3 nm from a neon charge exchange pumped sputtering copper hollow cathode laser. The line width of all of these emission lines is less than 0.1 cm^{-1}. The lasers presented here differ significantly from other metal vapor lasers in that the metal vapor pressure is generated by sputtering of a metal cathode rather than by evaporation from a hot metal source. Hollow cathode metal ion lasers operate at room temperature, require no preheating or standby power, and emit laser output within about 20 μs after application of voltage to the laser tube. In our laboratory lasers with overall length of 56 cm and active gain length of 40 cm have been demonstrated to emit over 200 mW @ 224.3nm (HeAg), 500 mW at 248.6 nm (NeCu), 100 mW at 260.0 nm (NeCu), and 500 mW @ 270.3 (NeCu).

The lasers developed here for use in UV Raman microscopic spectroscopy require an average input power of 20 – 100 W and provide an average output of typically 0.5 - 1.0 mW. An advantage of hollow cathode laser technology over positive column lasers is that the discharge can be modulated with fast rise and fall time less than 5 μs. Therefore the output and input power can be varied in an approximate linear fashion to suit experimental requirements. For *in situ* non-destructive biosignature detection the lasers operate at 1% duty cycle to minimize heating effects. The pulse width of the laser output can be varied from a few microseconds to one millisecond or greater since the laser transitions are CW transitions and not inherently limited in pulse width.

Raman Spectroscopy - First demonstrated by Raman and Krishnan in 1928, this vibrational spectroscopy technique measures the frequency shifts produced by the inelastic scattering of light from a target molecule.[5] The high information content of these vibrational spectra, the nondestructive nature of the technique, and the ease of sample preparation make Raman spectroscopy extremely attractive for a wide variety of biochemical investigations.[6,7]

Raman spectra represent the frequency shift that occurs following the inelastic scattering of photons from a molecule. This inelastic scattering differs from the relaxation emission of fluorescence in that it is a single event and a real excited emission state is not induced. In Rayleigh scattering an incident photon with an electromagnetic field of frequency ν_i interacts with a molecular electron cloud to produce an oscillating dipole moment. If the accelerating charge produces electromagnetic radiation at an output frequency $\nu_o = \nu_i$ it is known as Rayleigh scattering. The scattering frequency can be modified when nuclear vibrational motion induces electron cloud oscillation at frequency ν_n. Coupling vibrations ν_i and ν_n produces a beat frequency at $\nu_i \pm \nu_n$. The resultant Raman scattering will appear as a frequency shift to the red (Stokes shift, $\nu_o > \nu_i$) or blue (anti-Stokes shift, $\nu_o < \nu_i$) in the emitted frequency. A shift to the red is to be expected unless the event occurs with a molecule in an excited state. In that case, excitation will result in a net loss of energy with the excited molecule relaxing to the ground state

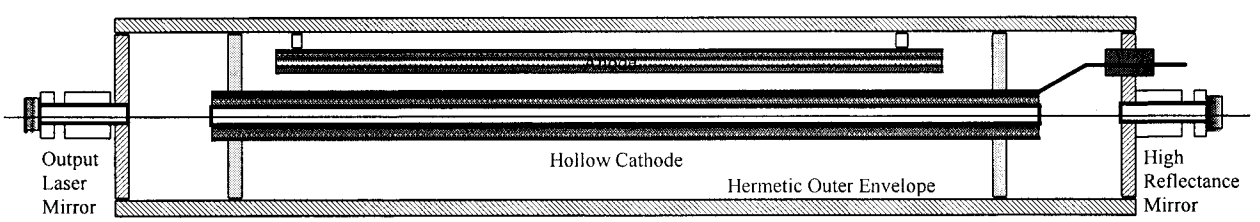

Figure 1. Schematic representation of a hollow cathode metal ion laser.

after emitting a higher energy photon.

Molecular electron clouds exhibit preferred frequencies of oscillation known as electronic absorption band frequencies. Excitation here produces a "resonant" effect with increased oscillating charge displacement and enhanced Raman scattering as high as 10^8. The most common form of resonance event results from a Franck-Condon enhancement of the molecular vibration. Here a component of the induced vibration is in a direction in which the molecule expands during an electronic excitation. The more the molecule expands along this axis during absorption of electromagnetic energy, the larger the enhancement factor. Common examples are the ring breathing (in-plane expansion) modes of the aromatic and nucleic acids. The degree of signal enhancement roughly follows the intensities of the absorption spectrum. [8]

Raman techniques have proven particularly useful in determining the molecular structure and dynamics of viruses producing information that rivals x-ray crystallographic experiments, but with comparatively little sample preparation.[9-17] Sample excitation in visible wavebands elicits characteristic Raman vibrational spectra for terrestrial soil and mineral samples.[18] The technique has been proposed for *in situ* mineralogical and paleontological exploration of the Martian regolith. [19,20]

Unfortunately, the Raman event is an inherently inefficient or photon-poor phenomena ($S/N < 10^{-9}$) with signal strength decreasing with excitation wavelength, ν_i, as a function of $1/ \nu_i^4$. That means excitation using longer wavelengths in the visible or near infrared demands either prolonged collection times or significantly increased power delivered to sample and power consumption. In addition, most complex biological molecules are Raman active at visible wavelengths. As a result, conventional Raman experiments in visible wavelengths produce, if not masked by fluorescence, a multitude of spectral lines, many of which are difficult to assign in a complex system.

One strategy for increasing both the strength and the selectivity of Raman analysis involves choosing an excitation wavelength that falls within the absorption band of a particular set of target molecules.[21] Reliance on the resonance event to achieve adequate signal to noise levels minimizes interference from neighboring potentially Raman-active molecular species with absorption bands distant from the exciting wavelength. Several biomolecules essential for bacteria and other living cells on this planet exhibit absorption bands in the deep ultraviolet (DUV). Under controlled laboratory conditions DUV laser excitation (220-260 nm) of the nucleic acids, aromatic amino acids, and quinones can produce selective Raman resonance events. This resonance response increases signal strength by as much as 10^8. As a result, several laboratories have used UV resonance Raman (UVRR) spectroscopy to investigate nucleic acids,[22,23] the secondary structure of DNA,[24-27] and the aromatic amino acids.[28-33] Selective UVRR has proven quite useful in monitoring alterations in oxidation state, electronic excited states, and peptide conformation.[34] The fact that UVRR spectroscopy may be the single most powerful technique for investigating protein secondary structure at low target molecule concentrations has inspired numerous investigations of proteins and polypeptides.[35-45]

Early attempts to produce non-resonant Raman spectra of bacteria with visible light excitation were unsuccessful due to fluorescence interference.[46-50] More recently excitation in the 200-257 nm range has successfully produced UV resonance Raman spectra for a variety of bacteria and spores.[52-57] Multivariate analysis can be used to extract sufficient information from high-resolution UVRR spectra to distinguish viruses, fungi, yeast, spores, gram negative and gram positive bacteria.[54] In fact, Nelson and colleagues have demonstrated the feasibility of producing reliable UVRR spectra from as few as 20 bacteria with 15 second integration times with excitation at 257.2 nm (2-3 mW delivered to sample and organisms cooled to minimize sample thermal degradation).[56]

Excitation at wavelengths below 250 nm makes it possible to produce Raman spectra shortwards of the native fluorescence activity encountered in biological material. Native fluorescent emission from the aromatic amino acids and the nucleic acids occurs considerably farther upstream than the Raman shift for excitation at wavelengths below 250nm. For excitation in the deep UV the entire Raman spectra appears typically within <10-15 nm of the excitation wavelength, while the native fluorescence emission of, for example, tryptophan appears between 300 and 500 nm.

This makes it possible to obtain both fluorescence and Raman information in a single experiment.

In the case of the three wavelengths chosen for this work, excitation at 325 nm produces a significant fluorescent response from a wide variety of organic molecular species making it useful as a preliminary scanning tool to locate regions of possible interest. However, non-specific fluorescent activity can be expected to obscure any Raman response. Excitation at 248.6 nm falls within the absorption bands for primarily the nucleic acids and to a lesser extent the aromatic amino acids. The resonance Raman response of bacteria to excitation at this wavelength is not obscured by fluorescence and derives primarily from interaction with these heterocyclic and aromatic ring structures. Excitation at 224.3 nm falls within the absorption bands for the aromatic amino acids. The bacterial resonance Raman response to excitation at this wavelength is even further removed from the upstream fluorescence activity and derives primarily from interaction of the incident light with the aromatic amino acids and to a lesser extent cytosine.

Native Fluorescence - Fluorescence remains the gold standard for efficient optical detection.[8,45] Most techniques involve tagging a target with a molecule possessing a significant fluorescence cross-section. Detection of native fluorescence following excitation in the deep UV remains a relatively unexplored arena. A central task for our instrument involves searching for localized targets including microorganisms on mineral surfaces. As outlined above, these organisms contain robust aromatic and heterocyclic ring compounds capable of native fluorescent response to deep UV excitation. It can be shown from an analysis of the predicted native fluorescent cross-sections (see below) that rapid (~1 second per field of view) detection of single microorganisms is quite feasible. Tryptophan absorbs well from 230-290 nm with a maximum occurring at ~275-280nm. Tyrosine absorbs well from 220-235 nm and from 265-285 nm with maxima at 230 and 275 nm. The nucleic acids exhibit strong absorption cross-sections from 245-275 nm. Emission spectra from these species peak between 300-400nm with significant activity occurring in visible wavelengths.

Summary – UV resonance Raman spectroscopy has proved increasingly useful as a non-invasive probe capable of detecting, classifying, and studying microorganisms in solution with minimal sample preparation. What has not been known prior to this investigation was whether or not a UVRR spectral signal characteristic of extant or extinct organic life as we know it could be obtained *in situ* in the presence of a potentially obscuring mineral matrix. To address this question we designed and constructed the current compact system incorporating UV native fluorescence imaging and Raman spectrometer operating at 224.3, 248.6, and 325 nm. We first describe the lightweight, low power consumption, deep UV air-cooled hollow cathode laser that has made this work feasible. We then outline the optical layout of the system. We illustrate the system's potential utility by presenting UVRR spectra for the gram negative iron reducing bacterium

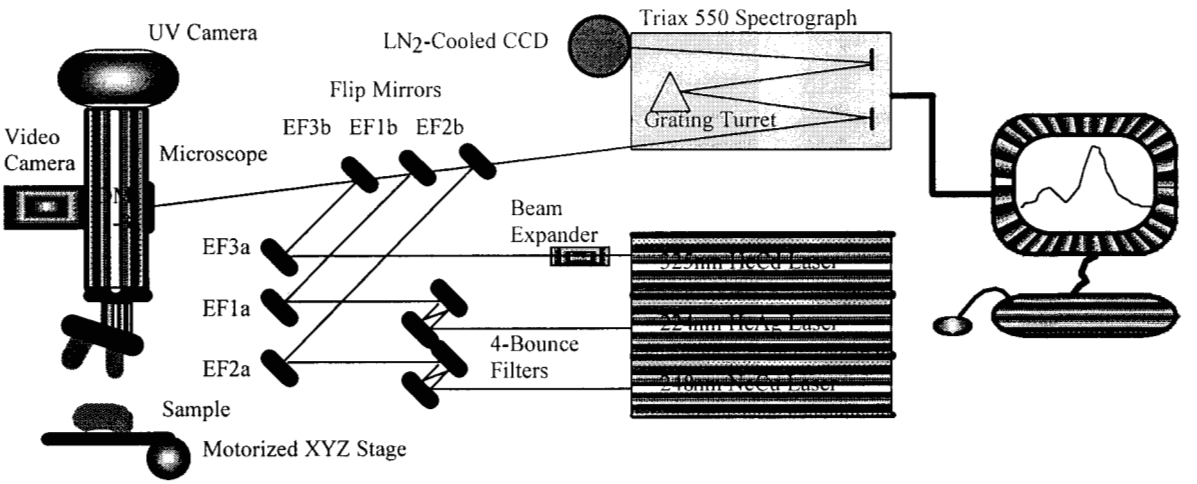

Figure 2. Optical layout of the deep UV native fluorescence imaging and resonance Raman spectroscopy system.

Shewanella oneidensis (MR-1) obtained *in situ* with the organism residing (a) on the unpolished surface of the mineral calcite and (b) in a medium-grained Mars soil analog. Finally, we present evidence that obtaining spectral data from native fluorescence active sites significantly enhances UVRR effective sensitivity when exploring a sparsely populated sample for clustered concentrations of organisms.

II. INSTRUMENTATION

Ultraviolet Lasers - The lasers used on this instrument produce emission wavelengths at 224.3, 248.6, and 325.0 nm with an oscillation bandwidth of less than 3GHz. Therefore, the limiting Raman resolution due to laser emission bandwidth is approximately 0.1 cm^{-1}. The 224.3 nm laser is a hollow cathode sputtering metal ion laser using a combination of helium and other noble gases as buffer gases and silver as the gain material (Photon Systems, Model HeAg60-224SL). The hollow cathode uses very pure silver on the inner diameter (Figure 1). The 248.6 nm laser is also a hollow cathode sputtering metal ion laser using a combination of neon and other noble gases as buffer gases and copper as the gain material (Photon Systems, Model NeCu60-248SL). The copper hollow cathode uses very pure copper on the inner diameter. The discharge geometry for both lasers is transverse with a brush-type anode located along most of the length of the 40 cm long by 3 mm inside diameter cathode.

Although the 224.3 nm and 248.6 nm emission lines are CW transitions, we operate these lasers in a chopped-CW fashion to reduce average input power and minimize the size and complexity of the laser tube and power supply. Optimum peak output is over 400 mW for NeCu laser and 100 mW for HeAg lasers with an operating duty cycle of about 1%. The average input power to the laser is less than 100 W. A power supply provides square wave voltage pulses to the cathode with a pulse width adjustable from about 30 μs to 500 μs. The corresponding drive current is also square wave and ranges in current from about 5A to 30A. Laser output commences within ~10 μs of voltage application. No warm-up or preheating of the laser tube is necessary. Each laser pulse is independent allowing the laser to operate in single pulse or multiple pulse mode. The laser can be also operated in extreme environments without the need for warm-up, preheating, or temperature regulation. The emitted laser beam is ~3 mm diameter with a divergence ~0.3mr. The longitudinal mode spacing is ~257 MHz. The transverse mode structure is multimode with the "times diffraction limit" of the beam about 18. Hence, these lasers can be focused to spot sizes of ~5 μm using an objective lens with NA = 0.5.

The 325.0 nm laser is a positive column metal vapor laser using helium as a buffer gas and cadmium as the active gain material (Melles Griot, P/N 3056-5). This laser requires a warm-up time about 5 minutes. Output of this laser is ~5 mW. The transverse mode is a Gaussian with a diameter of about 0.2 mm.

Optical Design - The UV Raman instrument is illustrated in Figure 2. It is composed of a spectrograph, a CCD array detector, three separate ultraviolet lasers, a microscope with multiple incoherent and coherent sources, a three axis motorized stage, a CCD video camera, a UV camera, and assorted lenses, spatial filters, edge filters, dichroic mirrors and other optics. The instrument was designed to allow excitation at three wavelengths in the ultraviolet. Excitation wavelength can be changed within a few seconds using flip mirrors and a dichroic mirror slide.

The optical path for each excitation wavelength is similar. At the output of the HeAg and NeCu lasers are multi-bounce edge filters employed to reduce plasma line emission from the lasers. The minimal plasma line emission of the HeCd laser makes possible the use of only a beam expanding lens pair.

After passing through the multi-bounce filter (or beam expander), the laser beam is reflected in tandem by two edge filters (Barr Associates), EFa and EFb. The edge filters are fabricated to efficiently reflect the laser wavelength and transmit at wavelengths immediately above the laser wavelength. Thus, EF1b is designed for 224.3 nm, EF2b for 248.6 nm and EF3b for 325.0 nm. These filters also assist in eliminating unwanted laser plasma emission lines. EFa and b are identical edge filters and are used in pairs to bring the laser beams into alignment with the optical path from the microscope axis into the entrance slit and along the spectrometer entrance axis. The EFb filters are mounted on flip-mirror assemblies (New Focus, P/N 9891) to allow rapid change of

excitation wavelength. After reflection by EFb, the laser beam is directed into the microscope. Within the microscope is a dichroic mirror slide containing three dichroic mirrors, DM1, DM2 and DM3, each designed to efficiently reflect, at 45 degrees, the laser line and a wavelength interval about 20 nm above the laser line. DM1 is for the 224.3 nm laser (CVI, P/N TLM1-240-45-1025), DM2 is for the 248.6 nm laser (CVI, P/N KRF-1025-45), and DM3 is for the 325.0 nm laser (CVI, P/N N-1025-45). Laser excitation wavelength can easily be selected by choosing the EFb and DM mirrors corresponding to the desired wavelength.

The microscope objective is a 40X ultraviolet refractive lens (Optics for Research, LMU-40) with effective focal length of 5 mm, working distance of 1 mm, NA of 0.50, and entrance aperture of 5 mm coated for UV between 224 nm and 325 nm with overall transmission of >92%. Calculated spot diameters at the sample for this lens are 2.85μ, 3.16μ, and 4.14μ for the 224 nm, 248 nm, and 325 nm lasers, respectively. The Rayleigh Range (R_r) defined as one half the depth of focus is the distance above and below the focal plane where the beam diameter has expanded to 1.414 times the minimal spot diameter and the power deposition per unit area is one half that at the focal plane. For 224 nm, 248 nm, and 325 nm the R_r = 28.5μ, 31.5μ, and 41.4μ, respectively. Power delivered to sample is 100 μW, 480 μW, and 330 μW, respectively.

The microscope axis is vertical with the laser beam reflected by one of the three DM mirrors, directed downward into the entrance aperture of the objective lens, and focused on the sample (Figure 1). Above DM is a microscope relay lens (Edmund Scientific, H37820) which images the sample onto a 768x494 element, 0.003 LUX, B/W CCD video camera (Watec, WAT-902B). Pixel size of the CCD camera is 8.4 μ (horizontal) x 9.8 μ (vertical). Spatial resolution of the CCD video camera is about 0.1 μ per pixel using the 40X refracting objective lens.

The camera produces images using either (1) broadband visible illumination in transmission or reflectance mode, or (2) laser illumination at 325.0, 248.6 or 224.3 nm. Broadband and laser illumination can be employed either independently or in concert. When employed concurrently the two visualization modes make it possible to locate fluorescent targets against irregular soil or mineral backgrounds. Using EFa and EFb mirrors, the laser beam spot can be centered in the middle of the video image.

Scattered light from the excited region on the sample is collected by the objective lens and collimated along the optical path to the spectrometer. The EF filters are employed to reject Rayleigh scattered light at the excitation wavelength. The remaining light, devoid of plasma lines and scattered light is then focused by L3 onto the entrance slit of the spectrograph. The diameter of the beam of scattered light from the sample is 8 mm, using the 40X refractive objective. To be compatible with the etendue (equals the product of the solid angle and aperture area) of the spectrometer, the focal length of L3 is 75 mm. With this lens, a minimum spectrograph slit width of about 125 μm is needed to eliminate light loss.

Table 1. Wavenumber coverage of the Spectrograph. Wavelength coverage depends on both excitation wavelength (224, 248, or 325 nanometers) and choice of grating (1800 or 3600 grooves per millimeter).

	Grating 1800 (3600) g/mm	
λ	Resolution/pixel	Single Capture
224 nm	2.78 (1.39) cm^{-1}	5686 (2844) cm^{-1}
248 nm	2.27 (1.13) cm^{-1}	4641 (2320) cm^{-1}
325 nm	1.32 (0.66) cm^{-1}	2702 (1351) cm^{-1}

The spectrograph is a 0.55 m, f/6.4 fully automated Czerny-Turner imaging spectrograph (Instruments SA, TR550MST1) with both 1800 g/mm and 3600 g/mm low stray light holographic gratings (76mm x 76mm each) in a computer controlled triple grating turret. The spectrograph employs computer controlled entrance slits and shutter. The CCD array detector assembly uses a 2048x512 array of 13.5 μm square pixels back illuminated and UV antireflection coated detector (English Electric Valve) temperature regulated and mounted in a liquid nitrogen cooled dewar (Instruments SA, Spectrum One CCD-2048x512-4). The dispersion of the spectrograph is 0.516 nm/mm with the 3600 g/mm grating and 1.032 nm/mm with the 1800 g/mm grating. With the above EEV CCD array detector the resolution is therefore 0.00697 nm per pixel using the 3600 g/mm grating and .01393 nm per pixel using the 1800 g/mm grating. The wavelength coverage in one capture is 14.27 nm with the 3600 g/mm and

28.53 nm with the 1800 g/mm grating (Table 1). The dark charge of this CCD detector is <1e/pixel/hour. Readout register full well capacity is typically 600,000 electrons and readout noise is typically 3 electrons rms.

To minimize total UV dose/unit time to sample we have implemented a motorized XYZ microscope stage moving the target material at a rate of 0.4 mm/second. Target trajectory can be either pre-programmed or altered in real time via computer interface (Newport Corporation, ESP6000 Unidrive6000) or manual over-ride depending on the demands of the experiment.

III. EXPERIMENTAL CONDITIONS

Initial measurements employed a gram negative bacteria *Shewanella oneidensis*, a facultative anaerobe ~1x2 microns in length common to many terrestrial and marine environments[58]. Cultures were grown in LB medium at room temperature in the microbiology laboratory of the Center for Life Detection (Jet Propulsion Laboratory, California Institute of Technology). Harvested cells were centrifuged and re-suspended in double distilled water to remove culture medium. Cell concentrations ranged from 10^6 to 10^8 cells/ml. Aliquots of these suspensions or dilutions of them were then added to mineral and soil backgrounds including a 1.0 X 1.2 cm unpolished calcite (calcium carbonate) crystal and granular palagonite.

On Earth calcium carbonate structures imply hydrothermal and sedimentary geological activity and make excellent environments for mixed colonies of microorganisms. Calcite exhibits a strong resonance Raman cross-section, scattering well at a variety of wavelengths. It has a principal peak at 1086-1088 cm^{-1}, and can exhibit accessory peaks at 713, 1435, and 1749 cm^{-1}.

The actual composition of Martian soil is as yet undetermined. Palagonite from Muana Kea Volcano in Hawaii represents the best known spectral analog to Martian soil[59-62] and was selected as the test soil for this experiment. It exhibits no native fluorescence or resonance Raman emission for the power densities and excitation wavelengths employed here.

Calcite samples were cleaned with triple ethanol washes and palagonite samples were baked at 500 °C. Baseline spectra were obtained at 325, 248, and 224 nm on all samples prior to inoculation with microorganisms. Wash and autoclave protocols were repeated if these spectra indicated contamination subsequent to cleaning. For the calcite experiment 20-80 μL aliquots of the bacterial suspensions were added to a 0.5 cm area on a moderately smooth calcite face. For the palagonite experiment similar aliquots were added to 80-100 mg of dry powdered palagonite, allowed to dry, and then mixed in a 0.5 cm diameter depression in a quartz microscope slide. Samples were visually scanned in video mode for evidence of localized laser induced native fluorescence response to 325nm, 248 nm, and 224 nm excitation. Frame rates were 1/30 second. UVRR spectra were obtained with excitation at 325, 248, and 224 nm. Power delivered to sample at each wavelength was 0.24, 0.33, and 0.14 mW, respectively. The lasers were defocused to minimize photodamage resulting in a spot size approximately 80 microns in diameter. Samples were taken both in scanning mode moving across the target area at 0.4 - 1.0 mm/second and as single area collections focused on fluorescing or non-fluorescing regions. No evidence of sample damage was detected in the collected spectra for scanning or single spot collections of one minute duration or less.

Spectra data collection times ranged from 10 to 60 seconds, with 30-60s sufficient to elicit reproducible spectra for bacterial samples. Data are displayed in counts per minute. Recording regions presented here are from 500 to 1800 cm^{-1}.

The exact manifestation of the resonance event and the assignment of vibrational bands depends on molecular ring breathing, stretch, and bending phenomena as well as secondary and tertiary structural effects. For the very low powers employed in this experiment a significant resonance enhancement must occur between important molecular pairs (including carbon-carbon double bonds, carbonyl bonds, and amides) and ring structures exhibiting an exceptionally large resonance Raman cross-section. The most common sources in microbial cells are the aromatic amino and nucleic acids. The assignments for the major bands characterizing the aromatic amino and nucleic acids have been well studied for UVRR with excitation wavelengths between 200 and 257 nm using both cw and pulsed lasers.[23,37-31,63] With minor exceptions the major bacterial spectral

contributions at the wavelengths employed in this study derive from the aromatic amino acids tryptophan and tyrosine plus three of the bases, adenine, guanine, and cytosine. Phenylalanine, thymine, and uracil exhibit cross-sections an order of magnitude smaller than these five molecules. Table 2 summarizes the most prominent bands characteristic of these target molecules for excitation between 223-229 nm and 244-248 nm.

Table 2. Assignments of Expected Strong Resonance Raman Bands Contributing to UVRR Spectra of *S. oneidensis* [1]

Molecule	Raman Band Assignment
Tryptophan	757-762[1] symmetric ring stretch of benzene and pyrrole 877-880 in-plane deformation **1006-1016** symmetric ring stretch of benzene and pyrrole 1340-1350 a pyrrole ring vibration **1549-1555** symmetric stretching of the indole ring 1614-1622 phenyl ring vibration
Tyrosine	830-832 Fermi resonance doublet 850-853 symmetric ring stretch **1178-1180** in-plane CH bend 1209-1210 symmetric stretch **1613-1617** in-plane ring stretching
Guanine[2]	1322-1326 (N7C8 s[3]; C8H b[4]) purine ring bonds **1485-1489** (C8H b; C8N9, N7C8 s) purine ring bonds 1575-1580 (N3C4, C4C5, C5N7 s) ring mode stretching 1603 (N1H b, C2N s) in-plane bending and ring stretching
Adenine	**1336-1339** (C5N7, N7C8 s) purine ring bonds 1482-1485 (C4N9 s, C8H b) purine ring bonds 1580-1581 (C4C5, N3C4 s) ring mode stretching
Cytosine	**1527-1528** (N3C4, N1C2 s) ring mode stretching 1650 (C2=O, C2N3 s) in-plane bending and ring stretching

[1]Raman band frequencies are in cm^{-1} units. Assignments, frequency ranges and nomenclature are from experimental and model compound studies.[23,27-31,63] Excitation was between 223-229 nm and 244-248 nm. [2]Nucleic acid studies employed nucleotides, deoxynucleosides, or the duplexes poly(rA)-poly(rU) and poly(dG-dC). Abbreviations signify Raman [3]stretching and [4]bending modes. The most prominent bands are in bold.

Tryptophan exhibits a particularly large cross-section for both native fluorescence and UV resonance Raman activity with both 248 and 224 nm excitation. Of particular importance are the bands at 757-762 cm^{-1} and 1006-1016 cm^{-1} deriving from the symmetric ring stretch of benzene and pyrrole rings within the indole structure. The band appearing between 877-880 cm^{-1} arises from an in-plane deformation. The 1340-1350 cm^{-1} band originating in a pyrrole ring vibration is particularly interesting since it is known to be sensitive to local environmental changes.[29] Symmetric stretching of the indole structure also produces the band at 1549-1555 cm^{-1}. The band appearing between 1614-1622 cm^{-1} arises from a phenyl ring vibration.

The most prominent tyrosine contribution is at 1613-1617 cm^{-1} and arises from in-plane ring stretching. Guanine and adenine exhibit quite similar activity between 1322-1339 cm^{-1} and 1485-1489 cm^{-1}. Both bands arise from stretching of purine ring bonds. Activity also occurs in both purines at 1580 cm^{-1} due to ring mode stretching. This bond is sensitive to base pair stacking and also offers a good example of the power of selective deep UV excitation. With 244-248 nm excitation the guanine contribution eclipses that of the adenine. Excitation between 223-229 nm produces the reverse response with the adenine contribution dominant.

The 765, 1007, 1344, and 1554 cm^{-1} bands elicited by 224 nm excitation can be assigned predominantly to tryptophan. The activity at 1186 cm^{-1} is most likely derived primarily from tyrosine while the 1600 cm^{-1} band is a combination of tryptophan and tyrosine with some minimal contribution from phenylalanine, adenosine, and guanosine. The 248 nm excitation bands at 1338 cm^{-1} can be assigned to adenosine. Both the 1427 cm^{-1} and 1604 cm^{-1} bands receive contributions from both guanosine and adenosine with some minimal contribution from tryptophan and tyrosine.

Nelson and colleagues have reviewed the assignment of vibrational bands in whole cell bacteria[56]. In both gram negative and gram positive organisms, prominent activity occurs between 1603 and 1615 cm^{-1} usually assigned to phenyl ring stretch of tryptophan and the in-plane ring stretching of tyrosine. For peaks closer to 1600 cm^{-1} some contribution by the 1603 cm^{-1} guanine band can be expected. Prominent bands appearing between 1482-1485 cm^{-1} and 1572-1575 cm^{-1} are assigned to purine ring bond activity of adenine and guanine. A band appearing frequently at 1336 cm^{-1} or beyond is assigned to adenine alone. Excitation between 222 and 229nm produces activity at 1180 cm^{-1} assigned to the in-plane CH bend of tyrosine and at the band at 1016 cm^{-1} is assigned

to symmetric stretch of benzene and pyrrole rings within the indole structure of tryptophan.

IV. RESULTS

Figure 3 depicts the UV Raman spectra for cleaned calcite and calcite inoculated with *S. oneidensis*. In Figure 3a Raman vibrational modes for calcite appear only at 1086 cm^{-1} for 325 nm excitation (fluorescence obscures the remaining modes). Activity appears at 713, 1086, 1430, and 1735 cm^{-1} for 248 nm excitation (Figure 3b) and at 1086 (primary), 1428, and 1725 cm^{-1} using 224 nm excitation (Figure 3c). At 325 nm excitation of calcite inoculated with bacteria (Figure 3d) all bacterial modes appear obscured in fluorescence with only the strong primary calcite line clearly resolved. Vibrational modes for *S. oneidensis* appear at 1338, 1427, and 1612 cm^{-1} for 248 nm excitation (Figure 3e) and at 765, 1007, 1186, 1344, 1554, and 1600 wavenumbers for 224 nm excitation (Figure 3f). The variation in peak locations produced by excitation at 224 and 248 nm reflects the selective nature of the resonance Raman experiment. For example, the shift between 1600 and 1612 cm^{-1} for 224 and 248 nm excitation respectively, may reflect a shift in relative resonance Raman cross-sections for the 1603 cm^{-1} tyrosine *v8b* mode. The relative increase in tyrosine cross-section with 224 nm excitation is also reflected in the appearance of the 1186 cm^{-1} band. The activity at 1007 cm^{-1} and 1554 cm^{-1} that appears during 224 nm excitation and is absent as expected at 248 nm excitation is assigned to tryptophan symmetric ring

To estimate instrument sensitivity for eliciting spectral signatures of microorganisms on the surface of calcite, 10-40 microliters of solutions ranging from 10^7 to 10^8 organisms/ml were placed in a 0.5 cm diameter region on a moderately smooth but unpolished face. Equal aliquots were placed on a standard microscope slide to perform direct cell counts since direct visual counting on the calcite surface was found to be unreliable. Cells were counted on the microscopic slides using both phase contrast and fluorescence images obtained with a standard laboratory epifluorescence microscope

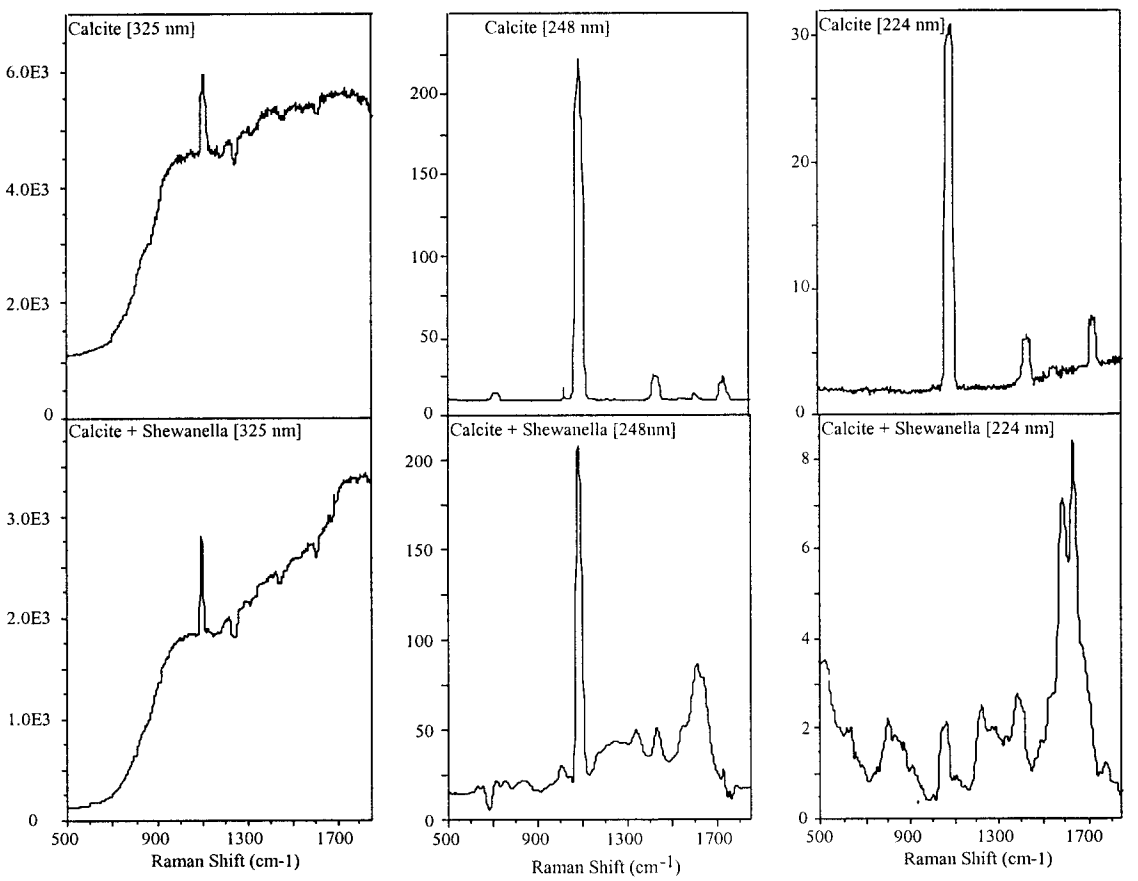

Figure 3. Ultraviolet (excitation at 325, 248, and 224 nm) resonance Raman spectra of calcite (a, b, and c) and calcite inoculated with the bacteria*S. oneidensis* (d, e, and f). Collection time is 60 seconds.

(Nikon, Eclipse E600) and then using confocal visible wavelength and fluorescence images from our test instrument. A >99% congruence for microorganism detection existed between the two broadband white light transmission techniques (phase contrast and confocal) and native fluorescence images. The detection of single organisms by native fluorescence imaging occurred in the test instrument with an effective field of view of ~2-5 X 10^3 μ^2 (50-80 μ laser beam diameter). Estimation of target area from the fluorescent clusters appearing on the calcite surface implied excitation of target physical cross-sections ranging from 20 to several hundred cells not counting layering effects (see below for a discussion of 2-D and 3-D organism density conversions

Scans of the inoculated calcite region elicited the strongest vibrational modes at 1600 cm^{-1} for 224 nm excitation and at 1612 cm^{-1} with 248 nm excitation. Peak heights were plotted as a function of the average number of organisms expected to fall within the excitation beam during scanning. Figure 4 demonstrates the expected signal fall off with dilution with complete loss of signal (for a one minute integration) occurring when cell densities fell below 5-10 cells per 100 square microns.

Of greater interest, however, was the variability of the signal strength regardless of dilution. Examination of visual and fluorescent microscopic images revealed a non-random distribution of microorganisms across the relatively rugged calcite surface. Bacteria tend to accumulate along crevasses in the mineral leaving a patchy target for the relatively small UV laser spot size (defocused to ~50 μ in diameter in this case). This phenomenon manifested in the inoculated samples mimics the behavior of microorganisms in natural environments with cells clustering in localized niches meeting specific nutrient, water, mineral, and energy requirements. As the distance between clusters of organisms increases with increasing dilutions the likelihood increases that a scanning probe either will lose signal strength while travelling along a barren valley or dramatically enhance the signal by accidentally traversing along a crevasse filled with organisms. Visual observation of fluorescent activity made it possible to collect spectra from both fluorescence-active and inactive regions. UVRR spectra obtained using 248 and 224 nm excitation of relatively non-fluorescing regions produced only the classical calcite modes, with no evidence of a biological signature (similar to spectra in Figures 3b and 3c). In contrast, the regions exhibiting clusters of native fluorescence activity yielded spectra compatible with the presence of microorganisms (similar to spectra in Figures 3e and 3f

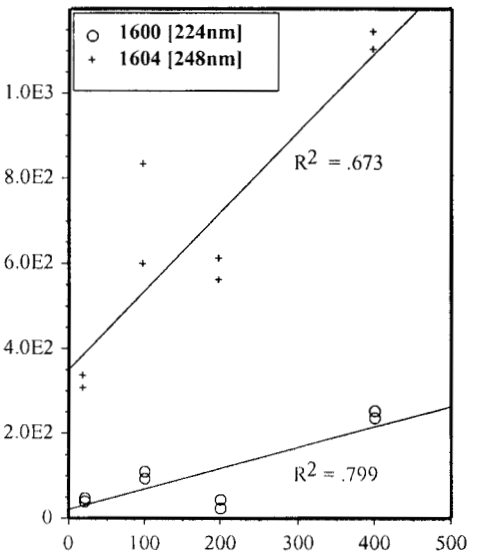

Figure 4. UV resonance Raman peak intensities as a function of te average number of bacteria expected ina 50m beam. Aliquots of cells were inoculated onto a natural calcite surface. Excitation occurred at 224 (o) and 248 nm (+).

A similar approach was employed with the Mars soil analog. Palagonite was inoculated with varying numbers of bacterial cells. Final soil concentrations of bacteria were calculated to range between 6 x 10^4 and 3 x 10^5 organisms/gm. Samples were then scanned with 325 nm and 248 nm excitation to identify fluorescing and non-fluorescing areas. Sufficient fluorescence emission occurs in visible wavelengths to allow identification of fluorescence rich or barren regions using real time video mode. 325 nm excitation produces fluorescent activity in a wide variety of bacterial components. Excitation at 248 nm elicits a significant resonance response from the nucleic acids, but the aromatic amino acids, dipicolinic acid, and some quinones also exhibit significant cross sections. Nucleic acids cross sections at 224 nm excitation are relatively weak. The activity at this wavelength can be attributed primarily to the aromatic amino acids. Ultraviolet photon energies are also significantly diminished at 248 nm compared to 224 nm thus

reducing saturation and photo-damage effects to target organisms. Damage effects are attenuated even more at 325 nm. As a result, searching for fluorescing regions is best done with the least destructive and most broadly informative probes (325 and 248 nm) employed first. Laser excitation at 224 nm is used to search selectively for the presence of aromatic amino acids.

Table 3. Dependence of UVRR signal strength for *S. oneidensis* on presence of fluorescence activity after 248 nm excitation. Varying quantities of the microorganism were inoculated into 80-100 mg of a palagonite Mars soil analog.[1]

Organism	Peak Intensity ($1604cm^{-1}$) with 248 nm Excitation (S/N)	
Cells/mg of Soil	Non-fluorescing Region	Fluorescing Region
305	10	55
94	5	75
62	7	235

[1]The UVRR signal at 1604 cm^{-1} appears in all samples, but proves dependent primarily on the presence or absence of localized fluorescence instead of on total number of organisms introduced. Peak intensities were converted to signal to noise ratios, i.e. S/N=10 implies the peak height is an order of magnitude greater than the noise level for this spectral region. Effective detection level is calculated as 6-30 x 10^4 cells/gm or 6-30 ppb of the palagonite samples.

Following classification of a region by its fluorescent activity Raman spectra were collected at all three wavelengths. While regional spectral differences appear at both 248 nm and 224 nm excitation, the 248 nm probe provided the richest and most robust signature. The 1604 cm^{-1} line is the strongest signal and probably derives primarily from tryptophan and tyrosine, but includes some contribution from guanine and cytosine species. All samples exhibited evidence of microorganism inoculation, but there was no significant correlation between the average organism concentration and signal strength when data were taken using a scanning strategy. When the search strategy changed to interrogating discrete fluorescing or non-fluorescing areas a clear pattern emerged. Table 3 compares the magnitude of the 1604 cm^{-1} line with estimated concentration of organisms per milligram of soil. While all areas gave evidence of organism inoculation, signal strength from fluorescing regions was 5 to 35 times stronger than the signal from fluorescence-free soil independent of

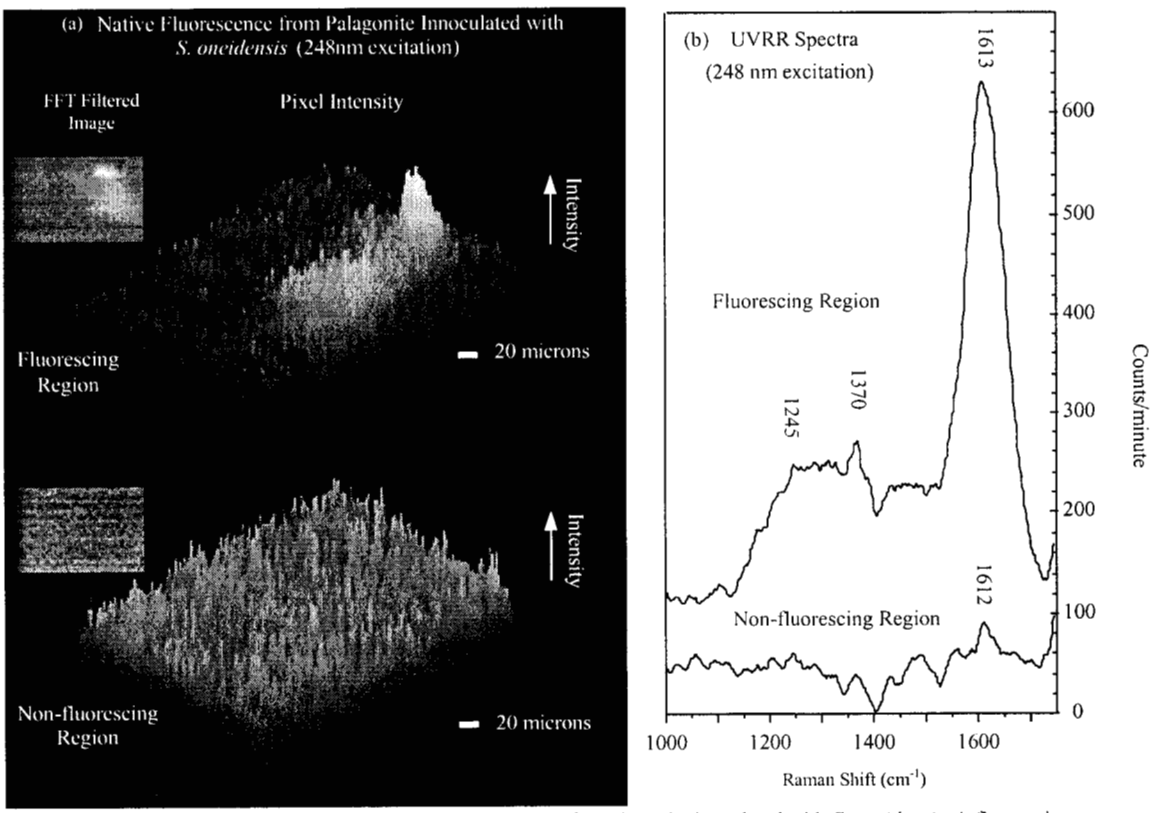

Figure 5. Native UV fluorescence and resonance Raman spectra for palagonite inoculated with *S. oneidensis*. A fluorescing region exhibits a significant increase in resonance Raman spectral S/N at 1612-1613 cm^{-1} when compared to a relatively non-fluorescing region. Excitation is at 248 nm and collection time was 60 seconds.

total organism concentration for the sample. Native fluorescence-active regions were observed to cover 10-20% of the laser spot size. We calculate that for a two dimensional tiling of organisms the majority of spectral information derives from between 20 and 40 cells located in the center of the excitation.

Figure 5 depicts the native fluorescence image (Figure 5a) and the accompanying UVRR spectra (Figure 5b) for a region of palagonite exhibiting native fluorescence and a non-fluorescing region. The region producing spatially localized native fluorescence yields a UVRR spectral signal strength some two orders of magnitude greater than the non-fluorescing portion of the sample. The data imply that rapid image scans of a sample to identify regions of native fluorescence can provide localized target areas appropriate for spectral data collection. Calculations derived from the number of cells added to the 80-100 mg of soil produce an effective detection in this study of 6×10^4 cells/gm or about 60 parts per billion (ppb) assuming a total weight for one microorganism $\sim 10^{-12}$ gm.[64]

IV. DISCUSSION

In broad terms the instrument has been designed as a high sensitivity, high resolution Raman microspectrometer. It can also provide visible and ultraviolet two-dimensional images of target regions using either incoherent broadband or coherent laser illumination. *In situ* geobiological exploration of extreme environments on Earth or elsewhere in the Solar System requires a probe capable of the non-destructive detection of organic chemical signatures against a variety of geological backgrounds. Ideally, this instrument could characterize spatially concentrated clusters of organic residues resident in natural soil samples as well as detect single microorganisms on a rock surface. Often during fieldwork here on Earth this is done using ultraviolet (UV) light that elicits fluorescence from aromatic compounds, and/or by adding fluorescent dyes that bind to biological materials. Unfortunately, the UV fluorescence absorption and/or excitation peaks of organic molecules are quite broad and contain minimal information content for accurate pattern recognition. In addition, the geological matrix may itself produce obscuring fluorescent activity. Fluorescent dye tagging works well for specific known targets, but is difficult to employ in extraterrestrial exploration of truly unknown geobiological environments. Certainly the fluorescence photons generated by the tagging molecule can obscure native spectral information.

The likelihood of detecting a single microorganism using only the native fluorescence response to deep UV excitation can be easily estimated. The photon flux produced by fluorescence from a single microorganism, ϕ, in photons/sec is given by

$$\phi = 5 \times 10^{15} \lambda I \sigma$$

where λ is the wavelength in nm, I is the incident excitation power density in W/cm^2, and σ is the total fluorescent scatter cross section in cm^2. If we assign the number of fluorescing molecules per organism, the fluorescence scattering cross section is estimated to be

$$\sigma = 10^{-20} \text{ cm}^2\text{/molecules} \times 10 \text{ molc/protein} \times 10^6 \text{ proteins/microbe}$$

[assumes 3 tryptophan + 7 tyrosine molecules/protein]

$$\approx 10^{-13} \text{ cm}^2\text{/microorganism}$$

For a laser with 0.1mW focused to a 10 μ diameter spot the excitation intensity is about $100 W/cm^2$. With this level of excitation the fluorescent yield from a single microorganism is expected to be about

Assuming an optical system collection efficiency of 10%, a spectrograph throughput of 10% and a quantum efficiency of the CCD array detector of 20%, there should be about 25,000 photoelectrons generated per microorganism. Even assuming the microorganism is smaller than one pixel of the CCD array, this will produce a signal substantially above the detector noise level and below the full bin saturation level for the detector. The rapid detection of a single microorganism should be quite feasible. These calculations point toward the possibility of developing a search strategy for microorganisms combining the sensitivity of UV fluorescence with the relative specificity of UVRR spectra.

In translating between the characterization of bacterial concentrations in the 3-dimensional space of solutions to the 2-dimensional surface experiment, a simple

thought experiment is instructive. A solution containing 10^8 microorganisms per milliliter distributes 10^8 cells in 10^{12} cubic microns. Each wall of the solution cube is a 10^4 x 10^4 micron grid containing 10^8 square microns. In an ideal 3D to 2D collapse 10^8 organisms each with a 1 square micron physical cross-section, would fully tile the 10^8 square micron floor of the 3D cube. This fully tiled state is the optimal geometric arrangement for the 2 dimensional UV native fluorescence or resonance Raman experiment. Most importantly this points out that total instrument sensitivity will be constrained by the match between beam spot size and target tiling. For the theoretical limit in the current system of a spot diameter of 3-4 microns only 3-13 cells with a 1 square micron cross-section are required to completely tile the beam area. It is important to note that photon density increases non-linearly from the perimeter to the center of the field of view.

We have demonstrated the existence of an easily elicited deep UV native fluorescence signal and UVRR organic signature from calcite and a Mars soil analog inoculated with the bacteria *Shewanella oneidensis*. The origin of both the native fluorescence activity and the UVRR signature can be tentatively assigned to bacterial nucleic and aromatic amino acids. Fluorescence detection prior to spectral interrogation markedly increases the sensitivity of the system. In current configuration a relatively diffuse large beam configuration has been employed (50-80 micron spot diameter) to diminish sample damage and increase the efficiency of wide area rapid (real time) scanning for evidence of clusters of native fluorescence. Obtaining spectra from these native fluorescent clusters sparsely dispersed in a soil sample produces effective detection limits for the spectral signature of tens of parts per billion. Laser spot size is diffraction limited making it theoretically possible to extract spectral information from a 3-5 square micron region. Focusing laser power in this fashion would permit the interrogation of a single organism, but at the cost of an increased likelihood of significant photodamage. Native fluorescence illumination and detection of a single organism using any of the three wavelengths in wide-beam mode appears quite feasible subject only to the presence or absence of background mineral fluorescent activity.

Other extreme environment targets for this system include residual pigments that remain following the death of a microorganism. These are often comprised of relatively insoluble organic ring structures, but typically derive from tryptophan, tyrosine, and/or phenylalanine. Native fluorescence imaging and wavelength selective Raman spectral interrogation of these difficult to analyze compounds could be the most direct observational technique available to us during extended extreme environment missions.

Extraterrestrial exploration demands instrumentation with low mass, low power consumption, low cost, and non-destructive characteristics. The enabling break-through for *in situ* use of native fluorescence and resonance Raman techniques in the deep ultraviolet is the hollow cathode sputtering metal ion laser. It is now feasible to fabricate deep UV lasers 10-15 cm in length, 2-4 cm in diameter, weighing 50-100 grams with an electronics package of comparable size, and drawing only 2-3 watts of electrical power. This technology opens up the possibility of developing a portable, potentially non-destructive, ultraviolet fluorescence imaging and Raman spectral probe for the geobiological exploration of natural environments.

AKNOWLEDGEMENTS

The authors would like to thank S. A. Asher, W. Nelson, H. Sun, and P. Conrad for useful discussions and R. Bhartia for assistance in sample preparation. This work was made possible by a grant from the Director's Research and Development Fund, Jet Propulsion Laboratory, California Institute of Technology and the National Aeronautics and Space Administration Astrobiology Grant.

REFERENCES

1. L. Csillag, M. Janossy, V. Rosa, and T. Salamon, Phys. Lett. A, **50**, 13 (1974).
2. D.C. Gerstenberger, R. Solanki, and G. Collins, IEEE J. Quantum Electr. **QE-16** (8), 820 (1980).
3. K. Jain, App. Phys. Lett. **34**, 39 (1979).
4. S.C. Wang, U.S. Patent No. 4,021,845, assigned to Xerox Corp., May 3, 1977.
5. C.V. Raman and K. S. Krishnan, Nature **121**(3048), 501 (1938).
6. *Biological Applications of Raman Spectroscopy*, edited by T. G. Spiro, Vol. I-III, (Wiley, New York 1987).
7. B. Hudson, Spectroscopy 1, **22** (1986)
8. P. R. Cary, *Biochemical Applications of Raman and Resonance Raman Spectroscopy* (Academic, New York, 1982).

9. S. A. Overman, M. Tsuboi, and G. J. Thomas, Jr., J. Mol. Biol. **259**, 331 (1996).
10. M. Tsuboi, S. A. Overman, and G. J. Thomas, Jr., Biochemistry **35**, 10403 (1996).
11. H. Takeuchi, M. Matsuno, S. A. Overman, and G. J. Thomas, Jr., J. Am. Chem. Soc. **118**, 3498 (1996).
12. R. Tuma, P. E. Prevelige, Jr., and G. J. Thomas, Jr., Biochemistry **35**, 4619 (1996).
13. R. Tuma, J.H.K. Bamford, D.H. Bamford, M.P. Russel, and G.J. Thomas, Jr., J. Mol. Biol. **257**, 87 (1996).
14. R. Tuma, J. H. K. Bamford, D. H. Bamford, and G. J. Thomas, Jr., J. Mol. Biol. **257**, 102 (1996).
15. T. Li, J. E. Johnson, and G. J. Thomas, Jr., Biophys. J. **65**, 1963 (1993).
16. K. E. Reilly and G. J. Thomas, Jr., J. Mol. Biol. **241**, 68 (1994).
17. R. Tuma and G. J. Thomas, Jr., Biophys. J. **71**, 3454 (1996).
18. A. Wang, B. L. Jolliff, L. A. Haskin, J. Geo. Res. Pla. **100**, 21189 (1995).
19. A. Wang, L. A. Haskin, and E. Cortez, Appl. Spect. **52**(4), 477 (1998).
20. A. Wang, B. L. Jolliff, L. A. Haskin, J. Geophys. Res. **104**, 27067 (1999).
21. S. A. Asher, Analytic. Chem. **65**(2) 59-66 (1993).
22. L. Chinsky, H. Hubert-Habart, A. Laigle, and P. Y. Turpin, J. Raman Spectrosc. **14**, 322 (1983).
23. S. P. A. Fodor, R. P. Rava, T. R. Hayes, and T. G. Spiro, J. Am. Chem. Soc. **107**, 1520 (1985).
24. M. Ghomi, R. Letellier, E. Taillander, L. Chinsky, A. Laigle, and P. Y. Turpin, , J.Raman Spectrosc. **17**, 249 (1986).
25. Y. Nishimura, M. Tsuboi, W. L. Kubasek, K. Banjor, and W. L. Peticolas, J. Raman Spectrosc. **18**, 221 (1987).
26. L. Chinsky, B. Jolles, A. Laigle, and P. Y. Turpin, J. Raman Spectrosc. **18**, 195 (1987).
27. J. R. Perno, C. A. Grygon, and T. G. Spiro, J. Phys. Chem **93**, 5672 (1989).
28. C. R. Johnson, M. Ludwig, and S. A. Asher, J. Am. Chem. Soc. **108**, 905 (1986).
29. S. A. Asher, M. Ludwig, and C. R. Johnson, J. Am. Chem. Soc. **108**, 3186 (1986).
30. M. Ludwig and S. A. Asher, J. Am. Chem. Soc. **110**, 1005 (1988).
31. S. P. A. Fodor, R. Copland, C. Grygon, and T. G. Spiro, J. Am. Chem. Soc. **11**, 5509 (1989).
32. J. Sweeny and S. A. Asher, J. Phys. Chem. **94**, 4784 (1990)
33, C. Su, Y. Wang, and T. G. Spiro, J. Raman Spectrosc. **21**, 8179 (1990)
34. S. A. Asher, Ann. Rev. Phys. Chem. **39**, 537 (1988)
35. R. P. Rava and T. G. Spiro, Biochemistry **24**, 1861 (1985).
36. S. Hashimoto, S. Ohsaka, H. Takeuchi, and I. Harada, J. Am. Chem. Soc. **111**, 8926 (1989).
37. G-Y. Liu, C. A. Grygon, T. G. Spiro, Biochemistry **28**, 5046 (1989).
38. R. G. Efremov, A. V. Feofanov, N. N. Modyanov, and I. R. Nabiev, FEBS Lett., **260**, 257 (1990).
39. J. B. Ames, S. R. Bolton, M. M. Netto, R. A. Mathies J. Am. Chem. Soc. **112**, 9007 (1990).
40. I. Harada, T. Yamagishi, K. Uchida, and H. Takeuchi, J. Am. Chem. Soc. **112**, 2443 (1990).
41. M. Netto, S. Fodor, and R. Mathies, Photochem. Photobiol. **52**, 605 (1991).
42. A. Toymana, E. Kurashiki, Y. Watanabe, H. Takeuchi and I. Harada, J. Am. Chem. Soc. **113**, 3615 (1991).
43. S. A. Asher, P. J. Larkin, J. Teraoka, Biochemistry **30**, 5944 (1991).
44. K. R. Rodgers, C. Su, S. Subramanian, T. G. Spiro, J. Am. Chem. Soc. **114**, 3697 (1992).
45. S. A. Asher, Analytic. Chem. **65**(4) 210 (1993).
46. J. Webb, Phys. Rep. **60**, 210 (1980)
47. L. Furia and O. P. Gandi, Phys. Lett. A **102**, 380 (1984).
48. S. Kinoshita, K. Hirata, and T. Kushida, J. Phys. Soc. Jpn. **49**, 314 (1980)
49. R. A. Dalterio, W. H. Nelson, D. Britt, J. Sperry, D. Psaras, J. F. Tanguay, and S. L. Suib, Appl. Spectrosc. **40**, 86 (1986).
50. R. A. Dalterio, W. H. Nelson, D. Britt, J. Sperry, D. Psaras, J. F. Tanguay, and S. L. Suib, Appl. Spectrosc. **41**, 234 (1987).
51. R. A. Daltario, W. H. Nelson, D. Britt, and J. F. Sperry, Appl. Spectrosc. **41**, 417 (1987).
52. K. A. Britton, R. A. Dalterio, W. H. Nelson, D. Britt, and J. F. Sperry, Appl. Spectrosc. **42**, 782 (1988).
53. R. Manoharan, E. Ghiamati, R. A. Dalterio, W. H. Nelson, D. Britt, and J. F. Sperry, J. Microbiol. Methods 11, 1 (1990).
54. W. H. Nelson, R. Manoharan, and J. F. Sperry, Appl. Spectrosc. Rev. **27**, 67 (1992).
55. S. Chadha, R. Manoharan, P. Moenne-Loccoz, W. H. Nelson, W. L. Peticolas, and J. F. Sperry, Appl. Spectrosc. **47**, 38 (1993).
56. S. Chadha, W.H. Nelson, J.F. Sperry, Rev. Sci. Inst. **11**, 3088 (1993).
57. G. P. Harhay and F. R. Siragusao., J. Rap. Met. Auto. Micro. **7**, 25 (1999).
58. K. Venkateswaran, D. P. Moser, M. E. Dollhopf, et al., Int. J. System. Bacter., 49, 705, Part 2 (1999).
59. C. R. Stoker and M. A. Bullock J. Geophys. Res. **102**(E5), 10881 (1997)
60. P. Toulmin, III, A.K. Baird, B.C. Clark, K. Keil, H.J. Rose Jr., R. P. Christian, P.H. Evans, and W.C. Kelliher J. Geophys. Res. **82**, 4625 (1977)
61. L.A. Soderblum and D.B. Wenner Icarus **34**, 622 (1978)
62. R.B. Singer J. Geophys. Res. **87**, 10159 (1982)
63. Z. Wen, S. A. Overman, and G. J. Thomas, Jr., Biochemistry **36**, 7810 (1997)
64. J. Ingraham, O. Maaloe, and F. Neidhardt, *The Growth of the Bacterial Cell*, (Sinauer, Assoc., Sunderland, MA, (1983).